

Identification of the roles of conserved charged residues in the extracellular domain of an epithelial sodium channel (ENaC) subunit by alanine mutagenesis

Oded Edelheit, Israel Hanukoglu, Nathan Dascal and Aaron Hanukoglu

Am J Physiol Renal Physiol 300:F887-F897, 2011. First published 5 January 2011;
doi:10.1152/ajprenal.00648.2010

You might find this additional info useful...

This article cites 41 articles, 18 of which can be accessed free at:

<http://ajprenal.physiology.org/content/300/4/F887.full.html#ref-list-1>

Updated information and services including high resolution figures, can be found at:

<http://ajprenal.physiology.org/content/300/4/F887.full.html>

Additional material and information about *AJP - Renal Physiology* can be found at:

<http://www.the-aps.org/publications/ajprenal>

This information is current as of April 7, 2011.

Identification of the roles of conserved charged residues in the extracellular domain of an epithelial sodium channel (ENaC) subunit by alanine mutagenesis

Oded Edelheit,^{1,2} Israel Hanukoglu,¹ Nathan Dascal,³ and Aaron Hanukoglu^{2,4}

¹Department of Molecular Biology, Ariel University Center, Ariel; Departments of ²Pediatrics and ³Physiology and Pharmacology, Sackler Medical School, Tel Aviv University, Tel Aviv; and ⁴Division of Pediatric Endocrinology, E. Wolfson Medical Center, Holon, Israel

Submitted 3 November 2010; accepted in final form 4 January 2011

Edelheit O, Hanukoglu I, Dascal N, Hanukoglu A. Identification of the roles of conserved charged residues in the extracellular domain of an epithelial sodium channel (ENaC) subunit by alanine mutagenesis. *Am J Physiol Renal Physiol* 300: F887–F897, 2011. First published January 5, 2011; doi:10.1152/ajprenal.00648.2010.—Epithelial sodium channels (ENaC) are composed of three homologous subunits whose extracellular domains (ECD) form a funnel that directs ions from the lumen into the pore of ENaC. To examine the roles of conserved charged residues (Asp, Glu, Arg, and Lys) on ECD, we mutated 16 residues in human α -ENaC to alanine. The modified cRNAs were expressed in *Xenopus laevis* oocytes together with wild-type β - and γ -ENaC. The effect of each mutation was examined on three parameters: amiloride-sensitive Na^+ conductance (assayed by the two-electrode voltage-clamp method), Na^+ -dependent self-inhibition of ENaC, and oocyte cell surface expression of ENaC (quantitated by confocal microscopy of yellow fluorescent protein linked to γ -ENaC). Mutation of 13 of 16 residues reduced the ENaC Na^+ conductance (to 40–80% of WT). Mutation of only six residues showed a significant effect on the Na^+ self-inhibition time constant (τ). All 16 mutants showed a strong correlation between ENaC activity and oocyte surface expression ($r = 0.62$). Exclusion of four mutants showing the greatest effect on self-inhibition kinetics (Glu250 and Arg350 with $\tau = \sim 30\%$ of WT, and Asp393 and Glu530 with $\tau = \sim 170\%$ of WT) increased the correlation to $r = 0.87$. In the ASIC1 homotrimeric model, the homologs of α -ENaC Asp400 and Asp446 are exposed on the protein surface far from the other two chains. The mutations of these two residues showed the strongest effect on cell surface expression but had no effect on self-inhibition. Control mutations to a homologous charged residue (e.g., Asp to Glu) did not significantly affect ENaC activity. Changes in the two parameters, Na^+ self-inhibition and oocyte surface expression level, accounted for the magnitude of reduction in ENaC activity as a result of the mutation to Ala. These results establish that while some conserved charged residues are part of the structure responsible for Na^+ self-inhibition, most are essential for transport to the oocyte cell surface.

cell surface; membrane; oocyte; self-inhibition

EPITHELIAL SODIUM CHANNELS (ENaC) are located at the apical membrane of epithelial cells where their major function is to funnel Na^+ ions from the lumen into the cell. Sodium ions that enter the epithelial cells via ENaC are then pumped out into the interstitial space via Na-K-ATPase located on the opposite basolateral membrane (25).

ENaC is composed of three homologous subunits named as α , β -, and γ -ENaC that are 669, 640, and 649 residues long,

respectively (28, 31). Each subunit has two transmembrane segments that are embedded in the apical membrane. The extracellular domains (ECD) of the three subunits of 456, 461, and 465 residues, respectively, are exposed on the lumen side of the membrane, forming a funnel that directs ions from the lumen into the pore of ENaC, and from there into the epithelial cell. The crystal structure of a homologous acid-sensing ion channel 1 (ASIC1) shows a homotrimeric complex (16). In view of this model, it is likely that ENaC functions as a heterotrimer composed of α , β -, and γ -ENaC (37). Both molecular genetic studies in humans (7, 11, 38) and in vitro expression studies (6, 12, 13, 31) indicate that all three subunits are essential for ENaC activity.

All the hereditary mutations that have been reported in the gene encoding for the α -ENaC subunit (SCNN1A) are associated with multisystem type I pseudohypoaldosteronism (PHA) (11). This is a severe salt-wasting disease that can lead to neonatal death, if not diagnosed and treated early (12, 14). Most of these mutations have been observed in the region coding for the ECD of ENaC.

We undertook the present study to examine the functional roles of conserved charged residues in the ECD of ENaC. Charged residues in proteins may have diverse roles including enhancing the hydrophilicity of the protein in an aqueous environment (4, 42), participation in the formation of intra- and intermolecular salt bridges between residues carrying opposite charges (e.g., Asp \leftrightarrow Arg) in interacting segments of proteins (19, 23, 27) and specific binding of ions during the course of ion movement in channels (20, 35, 40). Specifically in α -ENaC, charged residues have been shown to be essential for recognition by specific proteases that activate ENaC (18), and histidine residues in ECD have been shown to affect Na^+ dependent self-inhibition of ENaC (32).

Conserved residues on the surface of ENaC could possibly play a role in the functioning of ENaC, at any level, starting from the trafficking of the subunits to the cell surface (5) and extending up to the process of ion movement within the fully assembled ENaC on the cell surface (22). To examine the significance of these residues, we mutated each to alanine that carries no charge. The in vitro transcribed cRNAs generated from these cDNAs were then expressed in *Xenopus laevis* oocytes together with wild-type (WT) β - and γ -ENaC subunits and ENaC activity was assayed by the two-electrode voltage-clamp method.

Assay of ENaC activity by the two-electrode voltage-clamp method reports whole cell current that reflects both the number of the channels (N) in the membrane and the open probability

Address for reprint requests and other correspondence: I. Hanukoglu, Dept. of Molecular Biology, Ariel Univ. Center, Ariel 40700, Israel (e-mail: mbiochem@gmail.com).

Table 1. PCR primer sets used for cloning ENaC cDNAs from total cDNA reverse transcribed from human lung mRNA

Subunit	Primer Set	Forward	Reverse	Product, bp
α	RNA A	gagcaggacccttagacctctg	agcccttaccatcttctgctt	2,199
β	RNA B	tcccagtggtcaccacaactc	ttcaggaccaggatcaggac	2,310
γ	RNA G	cgagagcgagcagaggag	agtcctcactctggccttca	2,365

ENaC, epithelial sodium channel.

of the channel (P_o). Consequently, mutations of the residues would be expected to affect whole cell current by altering either cell surface expression of ENaC or the process of Na^+ conductance by ENaC. To distinguish between these two possibilities, we examined two parameters for each mutant: cell surface density of expressed ENaC and Na^+ self-inhibition of ENaC. Previous studies have shown Na^+ self-inhibition is associated with a reduction in channel P_o (33).

To measure the cell surface density of ENaC, we used a hybrid construct of γ -ENaC subunit and yellow fluorescent protein (YFP). To examine the functioning of Na^+ conductance by ENaC, we assayed rapid Na^+ -dependent self-inhibition of ENaC (9, 32–34). Our results show that the two parameters examined together account for most if not all of the reduction in ENaC conductance as a result of conserved residue mutations to alanine. Thus the charged residues examined appear to be functionally important mainly for structural configuration that affects Na^+ self-inhibition and/or transport to the cell surface.

METHODS

Plasmids. ENaC cDNA clones were generated from total human lung RNA as a template that was reverse transcribed using an RT-PCR kit (Promega) and oligo(dT) primer. The total cDNA was used as template for the synthesis of three specific cDNAs encoding for the α -, β -, and γ -subunits of human ENaC using the primer sets shown in Table 1. These cDNAs were then inserted into a pGEM-T Easy plasmid (Promega). For expression studies, we used pGEM-HJ, a version of the pGEM-HE vector (21). The inserts from the pGEM-T Easy plasmid were amplified by PCR using the primer sets shown in Table 2. The products of the PCR were cut with appropriate enzymes and subcloned into pGEM-HJ.

Site-directed mutagenesis. To examine the function of conserved charged residues by site-directed mutagenesis, we selected 16 residues that are conserved in all known sequences of α -ENaC from eight species (Table 3). These residues were modified to nonpolar alanine using a recently described site-directed mutagenesis method (10) with the primers listed in Table 4. As a control, we also generated additional mutant cDNAs wherein we changed the charged residue to another

charged residue with the following conversions: Asp \leftrightarrow Glu and Arg \leftrightarrow Lys. The primers used for generating these mutants are listed in Table 5. In Tables 4 and 5, we list only the forward primers. The reverse primers were complementary in sequence. After mutagenesis, we sequenced all isolated cDNAs using an ABI 310 Genetic Analyzer to ascertain that the cDNAs had the expected sequences without any additional change.

Electrophysiological measurements. The cDNAs were transcribed in vitro using T7-RNA polymerase (Promega) to generate cRNAs. The cRNAs (3 ng for each subunit) were micro-injected into immature stage V-VI *X. laevis* oocytes that were dissociated with 0.3 mg/ml type 1A collagenase. The method of preparation of the oocytes was approved by the Institutional Animal Care and Use Committee (permit no. 11–05-064). The oocytes were incubated at 19°C in ND-96 medium (in mM: 96 NaCl, 2 KCl, 1 CaCl₂, 1 MgCl₂, and 5 HEPES, pH 7.4) containing 2.5 mM sodium pyruvate, 50 μ g/ml gentamicin, and 10 μ M amiloride. ENaC-dependent amiloride-sensitive whole-cell inward Na^+ current was measured 2–3 days after cRNA injection using the two-electrode voltage-clamp method, while oocytes were clamped at -80 mV and continuously perfused with ND-96+10 μ M amiloride and ND-96 alternately at room temperature (20–25°C). Data were collected and analyzed using pClamp software (Axon Instruments).

Assay of Na^+ self-inhibition. The Na^+ -dependent self-inhibition of ENaC expressed in *X. laevis* oocytes was assayed following previously reported protocols. Oocytes were initially maintained in ND-96 medium. Each oocyte was injected with 1 ng cRNA for each of the three ENaC subunits. Within 30–60 min after injection, the perfusion medium was changed to NaCl-1 medium (ND-96 medium with 1 mM NaCl and 95 mM *N*-methyl-D-glucamine instead of 96 mM NaCl), and oocytes were kept in this medium for 24 h. The measurements were carried out using the two-electrode voltage-clamp method while the oocytes were clamped at -60 mV. After the initiation of the clamp, current was recorded under three conditions: 1) basal current for 1 min in NaCl-1 medium; 2) Na^+ current for 2 min after switch of perfusion medium to ND-96 medium; and 3) amiloride-inhibited basal current for 1 min after switch of perfusion medium to ND-96+10 μ M amiloride. Self-inhi-

Table 2. PCR primer sets used for amplifying ENaC cDNAs from pGEM T Easy plasmids

Subunit	Primer	Sequence
α	pGEM-HJ BamH1-F	tacggatccatggagggggaacaagctggag
α	pGEM-HJ Xba1-R	taatctagatcaggcccccccagaggac
β	pGEM-HJ BamH1-F	tacggatccatgcacgtgaagaagtacctgct
β	pGEM-HJ Xba1-R	atatctagattagatggcatcaccctcactg
γ	pGEM-HJ BamH1-F	tacggatccatggcaccggagagaagatc
γ	pGEM-HJ Xba1-R	taatctagatcagagctcattccagcatctgg

Table 3. Conservation and roles of α -ENaC residues mutated

α -ENaC Residue	Conserved in Subunits	ASIC1 Homolog	Surface	Interface
Asp235	$\alpha\gamma$	—		
Glu250	$\alpha\beta\gamma$	—		
Arg333	α	Asp224	+	—
Asp338	$\alpha\beta\gamma$	Glu229	+	—
Arg350	$\alpha\beta\gamma$	Lys247	+	A-C
Glu358	$\alpha\gamma$	Glu255	+	A-C
Asp393	α	Asp290	+	—
Asp400	$\alpha\beta\gamma$	Asp297	+	—
Asp446	α	Thr337	+	—
Lys474	α	Val361	+	—
Arg476	$\alpha\beta\gamma$	Glu363	+	—
Lys477	α	Met364	+	—
Arg518	α			
Glu530	α	Ala413	+	A-B
Lys534	$\alpha\beta\gamma$	Glu417	+	A-B
Glu538	$\alpha\beta\gamma$	Gln421	+	A-C

ASIC1, acid-sensing ion channel 1.

bition is strongly dependent on temperature. Thus all the experiments were carried out at room temperature strictly maintained at 22°C. We carried out the same experiments using LiCl instead of NaCl. LiCl-1 and LiCl-96 were used as the equivalent corresponding buffers for these experiments. The time constant (τ) was calculated by fitting the first 40 s of current decay with an exponential equation by Clampfit 10.1 (Axon Instruments).

Fluorescence measurements and detection of YFP expression in oocytes. To examine the oocyte membrane distribution of ENaC subunits, we generated a γ -ENaC-fluorescent protein fusion construct. For this, we amplified the coding sequence of YFP and inserted the PCR fragment at the *Bam*HI site after the γ -ENaC coding sequence in PGEM-HJ vector.

In experiments designed to determine fluorescence of γ -ENaC-YFP hybrid protein in oocyte membrane, 12 ng of cRNA was injected into oocytes. The oocytes were incubated in ND-96 medium with 10 μ M amiloride at 19°C for 3 days. The oocytes were then transferred with a pipette to ND-96 medium in a 0.7-mm glass-bottom dish for imaging using a confocal fluorescence microscope (Zeiss LSM 510 META,

Table 4. Forward primers used for mutation of charged residues to alanine by site-directed mutagenesis

Primer	Sequence
D235A-F	ccagaacaaatcggcctgctttctaccagacatac
E250A-F	ctgggatgcggtgagggcgctggtaccgcttccac
R333A-F	ctgtccctgatgctggccgcagagcagaatgac
D338A-F	cgcgagagcagaatgccttccattcccctgctg
R350A-F	caacagtactggggccgcggtaatggtgcacggg
E358A-F	gtgcacgggcaggatgcacctgcctttatggatg
D393A-F	ggggcgattatggcgctgcacctgcaacaaatggc
D400A-F	caccaagaatggcagtgctgttctctgttgagaac
D446A-F	gaacgtggagtactgtgcttacagaaagcacag
K474A-F	ctgggctgtttcaccgcgctgcccgaagccatgc
R476A-F	ctgtttcaccagtgctgcgcaagccatgcagctg
K477A-F	gtttcaccagtgcccggcgccatgcagcgtgacc
R518A-F	caccgtcaacaacaggcaaatggagtgcccaag
E530A-F	caacatcttcttcaaggcgetgaaactcaaaaacc
K534A-F	caaggagctgaactacgcaaccaattctgagtcctc
E538A-F	ctacaaaaccattctcgtctcctctgtcagc

Table 5. Forward primers used for conservative mutation of charged residues by site-directed mutagenesis

Primer	Sequence
D235E-F	gcaaccagaacaaatcggagtgcttctaccagac
R333K-F	ctgtccctgatgctgaaggcagagcagaatgacttc
E358D-F	gtgcacgggcaggatgatcctgctttatggatg
D393E-F	ggggcgattatggcgagtgccaccaagaatggc
D446E-F	gaacgtggagtactgtgagtagacaaaagcacagttc
K474R-F	ctgggctgtttcaccaggtgcccgaagccatgc
R476K-F	ctgtttcaccagtgcaagaagccatgcagcgtg
K477R-F	gtttcaccagtgcccgaaggccatgcagcgtgacc

Jena, Germany) with either $\times 5$ or $\times 20$ air objectives. YFP fluorescence was excited using a 514-nm argon laser line. The emission spectrum was recorded with a filter in the range of 524–609 nm.

The intensity of YFP fluorescence showed no significant variation at the animal (dark) hemisphere. For each oocyte, the fluorescence intensity was taken as the average of three points on the membrane, minus the average of three points inside the dark (nontransparent) part of the animal hemisphere using Zeiss LSM Image Examiner Software (version 4.2).

Immunoprecipitation of α -ENaC subunit. For determination of the relative amount of the expressed α -ENaC subunit, 12 ng of α -ENaC cRNA was injected into oocytes. The oocytes were incubated in ND-96 medium with [³⁵S]methionine (150 μ Ci/ml) at 19°C for 3 days. Oocytes were then homogenized in groups of 10 in 0.5 ml of homogenization buffer (in mM: 20 Tris, pH 7.4, 5 EDTA, 5 EGTA, 100 NaCl) containing Complete Protease Inhibitor Cocktail at a dose recommended by the manufacturer (Boehringer Mannheim) and centrifuged for 10 min at 700 g. The supernatant was removed, and CHAPS detergent was added to a final concentration of 1% and shaken at room temperature for 30 min. The supernatant was then centrifuged for 15 min at 13,000 g. The supernatant was removed and incubated with 4 μ l anti- α -ENaC (sc-21012, Santa Cruz Biotechnology) overnight at 4°C. The solution was reacted with 30 μ l protein A Sepharose CL-4B (GE Healthcare) with gentle shaking for 1 h at 4°C and centrifuged for 10 min at 700 g. The pellet containing the beads was washed three times with homogenization buffer. The beads were then suspended in gel sample buffer, heated for 5 min at 65°C, and precipitated by centrifugation. The clear supernatant was removed and electrophoresed in 6% polyacrylamide gel.

Software for analysis of sequence and structural homology. Multiple sequence alignment for the identification of conserved or homologous residues was carried out using Clustal software (8). Clustal results were visualized using GeneDoc (<http://www.nrbsc.org/gfx/genedoc/>) (24). Structural comparisons between human α -ENaC and the ASIC1 model (16) were limited only to regions showing unequivocal sequence homology. ENaC was also modeled using the SWISS-MODEL server (2). Molecular models were visualized using Discovery Studio Visualizer (Accelrys).

Statistical analysis. The activity of each mutant cRNA was tested in at least two independent experiments with at least 10 oocytes. Measurements were carried out without knowledge of the injected cRNA. Significance of the difference between means was analyzed first by one-way analysis of variance. Significance of the difference for subsequent multiple compar-

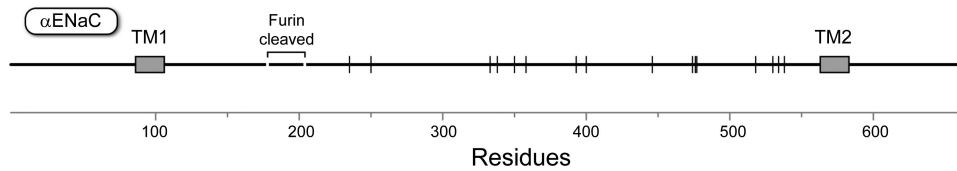


Fig. 1. Positions of the conserved charged residues mutated in the primary structure of the human α -epithelial sodium channel (ENaC) subunit. TM1 and TM2 mark the 2 transmembrane segments of the protein. The N and the C termini are located in the cytoplasm, and the portion between TM1 and TM2 is the extracellular domain.

isons between each mutant group vs. the control WT sample mean was tested by Dunnett’s test.

RESULTS

To select conserved charged residues in the extracellular domain of the α -ENaC subunit, we aligned all known sequences of α -ENaC from eight species (human, bovine, guinea pig, mouse, rat, rabbit, chicken, and *X. laevis*). The amino-terminal segment of α -ENaC is cleaved by cellular proteases such as furin (1, 18, 26). Therefore, we selected residues between the furin cleavage site and the second transmembrane domain of α -ENaC (Fig. 1). Some of the residues we selected are conserved also in β - and γ -subunits of human ENaC, as indicated in the second column of Table 3.

Mutation of charged residues to Ala inhibits ENaC activity. To examine the importance of the charged residues, we generated 16 different α -ENaC cDNAs where alanine was substituted instead of the selected charged residues. The cRNA coding for each mutated α -ENaC subunit was microinjected into *X. laevis* oocytes together with WT β - and γ -subunits. The oocytes were incubated for 2–3 days in a solution containing 10 μ M amiloride to block the ENaC currents. During the recording session, the cells were held in amiloride-containing medium at a holding potential of -80 mV (see METHODS) using the two-electrode voltage-clamp method. The amiloride-sensitive whole-cell ENaC current was determined by perfusing the cell with amiloride-free solution. Expression of only β - and γ -subunits without α -ENaC showed no significant amiloride-sensitive Na^+ current. The expression of WT β - and γ -subunits

together with mutated α -ENaC generated significant Na^+ current, ranging from about -10 to -30 μ A.

In a series of experiments with each of the mutants, we observed that alanine substitution reduced ENaC currents down to 40% of the level observed with the WT α -ENaC subunit (i.e., $\sim 60\%$ inhibition) (Fig. 2). Only three mutations showed no significant inhibition (Glu358Ala, Arg476Ala, and Arg518). There was no apparent correlation between the degree of inhibition and the range of conservation of the residue across all three subunits. The average degree of inhibition by mutation of residues unique to α -ENaC was 63%, and the average degree of inhibition by mutation of residues conserved in all three subunits was 58%.

To examine whether mutations of the conserved residues to a homologous residue can affect the ENaC activity of the channel, we generated eight mutants wherein the charge of the residue was maintained, i.e., Asp \leftrightarrow Glu, or Arg \leftrightarrow Lys. The results showed no significant difference between the activity of the mutants and the WT ENaC (Fig. 3).

α -ENaC mutations do not affect total expression of mutated α -ENaC subunit. Most of the ENaC subunits expressed in an oocyte remain in pre-Golgi compartments, and only a small fraction is transported to the oocyte surface membrane (39). To examine the possibility that differential macroscopic current density of ENaC channels results from different levels of translation of the microinjected cRNAs, we measured the total amount of newly synthesized ENaC proteins for each of the mutants. The results of the experiment showed no significant differences between the mutants (Fig. 4).

Effect of α -ENaC mutations on Na^+ -dependent self-inhibition. Following previously established protocols (32, 34), we measured the time constant (τ) for self-inhibition of ENaC after rapid change in Na^+ concentration in the medium from 1 to 96

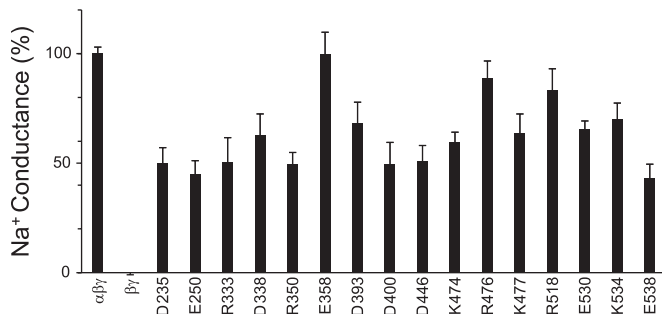


Fig. 2. ENaC Na^+ conductance in oocytes expressing an α -ENaC subunit with a charged residue mutated to alanine. Sodium conductance of oocytes injected with wild-type (WT) cRNAs for α -, β -, and γ -ENaC ($\alpha\beta\gamma$) was normalized to 100%. Control oocytes were injected with only cRNAs for β - and γ -ENaC ($\beta\gamma$). All other results represent Na^+ conductance in oocytes injected with an α -ENaC cRNA carrying a single residue (noted at the bottom of each bar) mutated to Ala and wild-type cRNAs for β - and γ -ENaC. The amiloride-sensitive sodium current was measured by the 2-electrode voltage clamp method 2 days after injection. Results shown are means \pm SE of at least 10 oocytes/mutation. For all mutants except for Glu358Ala and Arg476Ala, the mean was significantly different from the wild-type ($P < 0.05$).

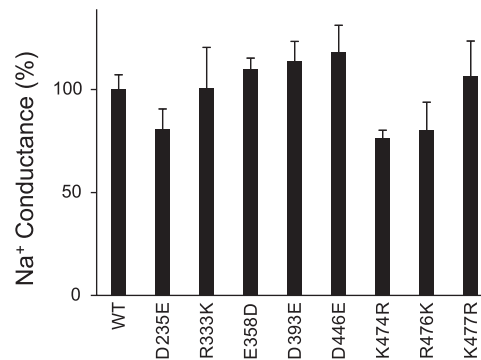


Fig. 3. ENaC Na^+ conductance in oocytes expressing an α -ENaC subunit carrying a charged residue mutated to a homologous residue, i.e., Asp \leftrightarrow Glu, Arg \leftrightarrow Lys. Values are means \pm SE of at least 10 oocytes/mutation. For other details, see METHODS and legend of Fig. 2.

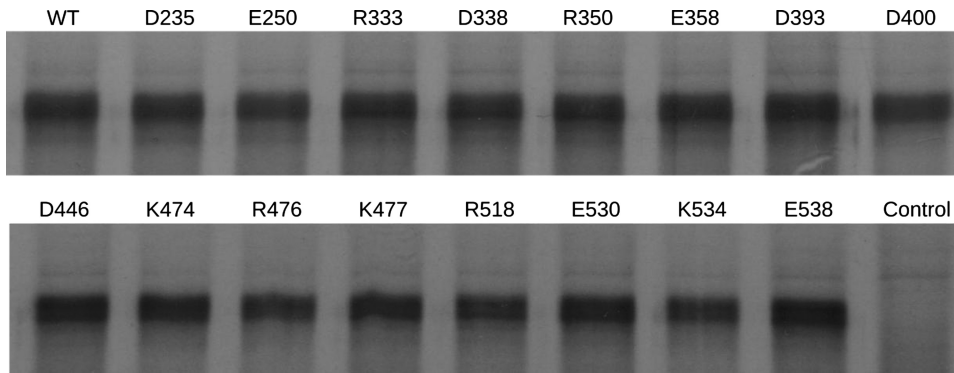


Fig. 4. Autoradiogram of WT and mutated α -ENaC protein expressed in oocytes immunoprecipitated using anti- α -ENaC antibody. Oocytes were microinjected with only α -ENaC cRNA and incubated with [35 S]methionine. After 3 days of incubation, proteins were precipitated with anti- α -ENaC antibody, separated by electrophoresis on a polyacrylamide gel, and autoradiographed. Control oocytes were not injected with α -ENaC cRNA.

mM as described in METHODS (Fig. 5). As previously noted, in Na^+ -dependent self-inhibition there is some variability between batches of oocytes. Therefore, in Fig. 6A the results are presented in percent values relative to the WT control oocytes recorded in the same experiment. The absolute τ values, in seconds, are presented in Supplementary Fig. S1A. Only eight of the 16 mutants showed τ values that were significantly different ($P < 0.01$) from the WT ENaC (Fig. 6A). Mutations of four residues (D235, E250, R350, and E538) to alanine caused a significant decrease in τ (i.e., accelerated self-inhibition), and mutations of two residues (D393 and E530) caused a significant increase in τ (i.e., decelerated self-inhibition) for Na^+ conductance change (Fig. 6A). The greatest reduction in τ

(to $\sim 30\%$ of WT) was observed for two mutants (E250A and R350A), and the greatest increase in τ (to $\sim 170\%$ of WT) was observed for two mutants (D393A and E530A) (Fig. 6A). When we carried out the same experiment with Li^+ instead of Na^+ , we obtained essentially the same results with no major difference from Na^+ -dependent self-inhibition (Supplementary Fig. S1B). Thus the WT ENaC and channels with alanine mutations showed the same quantitative response of self-inhibition with Li^+ as well as with Na^+ .

Na^+ dependent self-inhibition phenomenon has been previously assessed by an additional parameter based on the ratio of steady-state current (I_{ss}) and peak current (I_{peak}) observed after the rapid change of the bath medium to high Na^+ concentra-

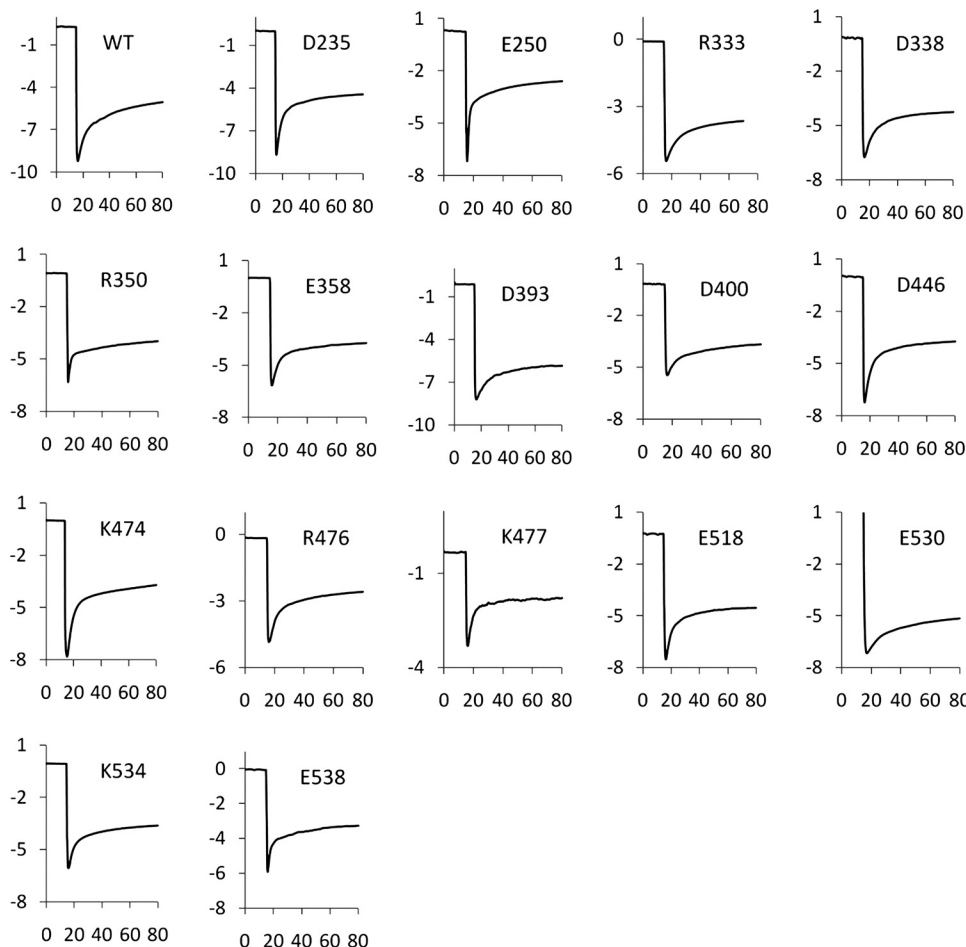


Fig. 5. Recordings of Na^+ -dependent self-inhibition response in oocytes expressing α -ENaC with WT β - and γ -ENaC subunits. The WT sample was injected with cRNAs encoding for α -, β -, and γ -ENaC subunits. All the other oocytes were injected with an α -ENaC cRNA carrying the mutation indicated. In each experiment, the oocyte was clamped at -60 mV and whole cell current was recorded while superfusing the oocyte with medium containing 1 mM NaCl (open bar). Na^+ concentration was then increased rapidly to 96 mM (gray bar). The time constant values shown in Fig. 6 were determined for a period of 40 s starting with the peak current (I_{peak}) response of each recording. I_{ss} , steady-state current.

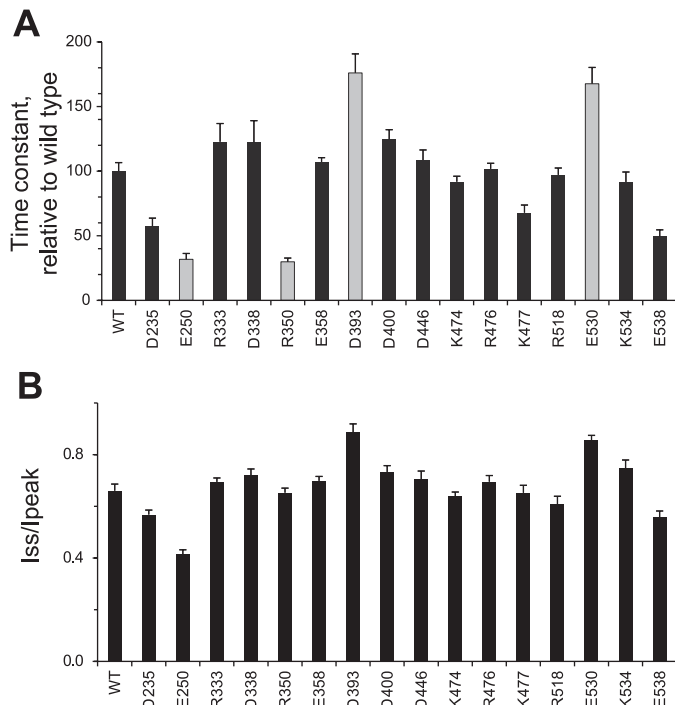


Fig. 6. Effect of mutations of conserved charged residues to alanine on Na⁺ self-inhibition of ENaC. A: time constant (τ) value relative to WT control oocytes of each batch. The time constant τ was calculated as noted in METHODS and Fig. 5. Each bar represents the mean \pm SE of at least 10 oocytes in at least 2 independent assays. Six mutants had τ values significantly different ($P < 0.01$) from the WT ENaC (D235, E250, R350, and E538 lower than WT and D393 and E530 higher than WT). The grey bars represent the 4 most significant differences from WT controls. B: I_{ss}/I_{peak} ratio. See Supplemental Fig. S1 for raw absolute time constant values for Na⁺ and Li⁺ self-inhibition.

tion. We measured the I_{ss}/I_{peak} ratio for all the mutants (Fig. 6B). The τ values and I_{ss}/I_{peak} ratios were strongly correlated for all 16 samples ($r = 0.865$) (Fig. 7). Such a correlation may indicate that Na⁺-dependent self-inhibition can be described as a reversible first-order process of the type $O \rightleftharpoons C$, where O is the open and C is the closed (Na⁺-inhibited) state of the channel. In this case, both the time course of self-inhibition and the steady-state level of the remaining current are generally determined by the ratio between forward (inhibition; $O \rightarrow C$) and backward (recovery; $C \rightarrow O$) rates, k_1 and k_{-1} , respectively. In such case, $\tau = 1/(k_1 + k_{-1})$ and $I_{ss}/I_{peak} = k_{-1}/(k_1 + k_{-1})$ (15). A simple case in which a linear relationship between τ and I_{ss}/I_{peak} (as shown in Fig. 7) may be observed occurs when the mutations change only k_1 whereas k_{-1} remains constant. In ENaC, which is normally constitutively active in the plasma membrane, the steady-state P_o will be linearly related to I_{ss}/I_{peak} ; therefore, changes in the latter are excellent indicators of changes in P_o caused by a mutation. Only one mutant (R350A) consistently showed a deviation from this behavior. In this mutant, the channel was closed rapidly but the steady-state I_{ss}/I_{peak} was reduced only slightly (cf. recordings in Fig. 5). The data point for R350A showed the largest deviation from the linear regression line (Fig. 7). This deviation could result from a change in more than one parameter of the self-inhibition process (e.g., both k_1 and k_{-1} are altered by the mutation), or from a recording artifact whereby the inhibition starts very rapidly and the I_{peak} value is underesti-

mated. Without this R350A mutant the correlation coefficient between τ and I_{ss}/I_{peak} ratios was $r = 0.93$ (Fig. 7).

Cell surface expression of ENaC subunits can be tracked using a γ -ENaC-YFP hybrid protein. To assay cell surface density of ENaC, we generated a hybrid protein constructed of γ -ENaC with YFP attached at its carboxy terminus. Expression of WT α - and β -ENaC together with γ -ENaC-YFP showed strong oocyte cell surface fluorescence that could be quantitated by confocal microscopy (Fig. 8). Expression of β -ENaC together with γ -ENaC-YFP showed low fluorescence ($\sim 14\%$ of that observed with $\alpha\beta\gamma$ -ENaC) (Fig. 9). Expression of γ -ENaC-YFP alone gave even lower fluorescence (2.3%). In contrast, expression of all mutated α -ENaC subunits showed detectable fluorescence at the oocytes' surface (Figs. 8 and 9).

Activity of ENaC reconstituted with mutated α -ENaC is correlated with the cell surface expression of ENaC. The results of Na⁺ self-inhibition analysis did not show a general correlation with the macroscopic conductance of the mutants. In contrast, oocyte surface fluorescence of ENaC showed a significant correlation with conductance of the mutants. The Pearson correlation coefficient between the two sets of values was $r = 0.62$ ($P < 0.01$). In other words, the results showed that ENaC conductance increases as a function of surface membrane density of ENaC.

If the mutation of a residue reduces single-channel Na⁺ conductance or P_o of ENaC channels, then it would also be expected to reduce general channel activity irrespective of channel density in the membrane. Thus the inclusion of such cases in the correlation between cell surface density vs. macroscopic Na⁺ conductance would be expected to reduce the overall correlation. The Na⁺-dependent self-inhibition experiments showed that some of the mutations affect ENaC activity independently of ENaC expression on the cell surface. Exclusion of the values for four mutants with the greatest effect on Na⁺ self-inhibition increased the correlation coefficient between the two sets of values to $r = 0.87$ ($P < 0.0001$) (Fig. 10). It should be noted that three of the four mutants had the largest residuals in the linear regression plot (Fig. 10).

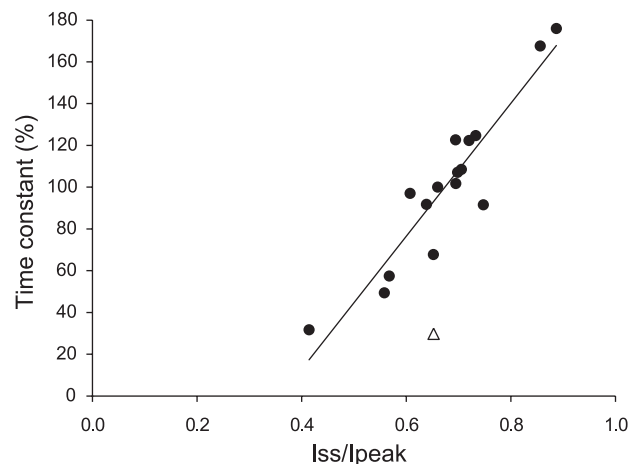


Fig. 7. Correlation between the time constant τ value and I_{ss}/I_{peak} ratios for the Na⁺ self-inhibition response of 16 α -ENaC subunits carrying a charged residue to alanine mutation. The correlation coefficient for all 16 samples was $r = 0.865$. The linear regression line was drawn for 15 points excluding 1 value (shown as a triangle) for mutant (R350A) because of its different behavior (see RESULTS). Without this point, the correlation coefficient was $r = 0.93$.

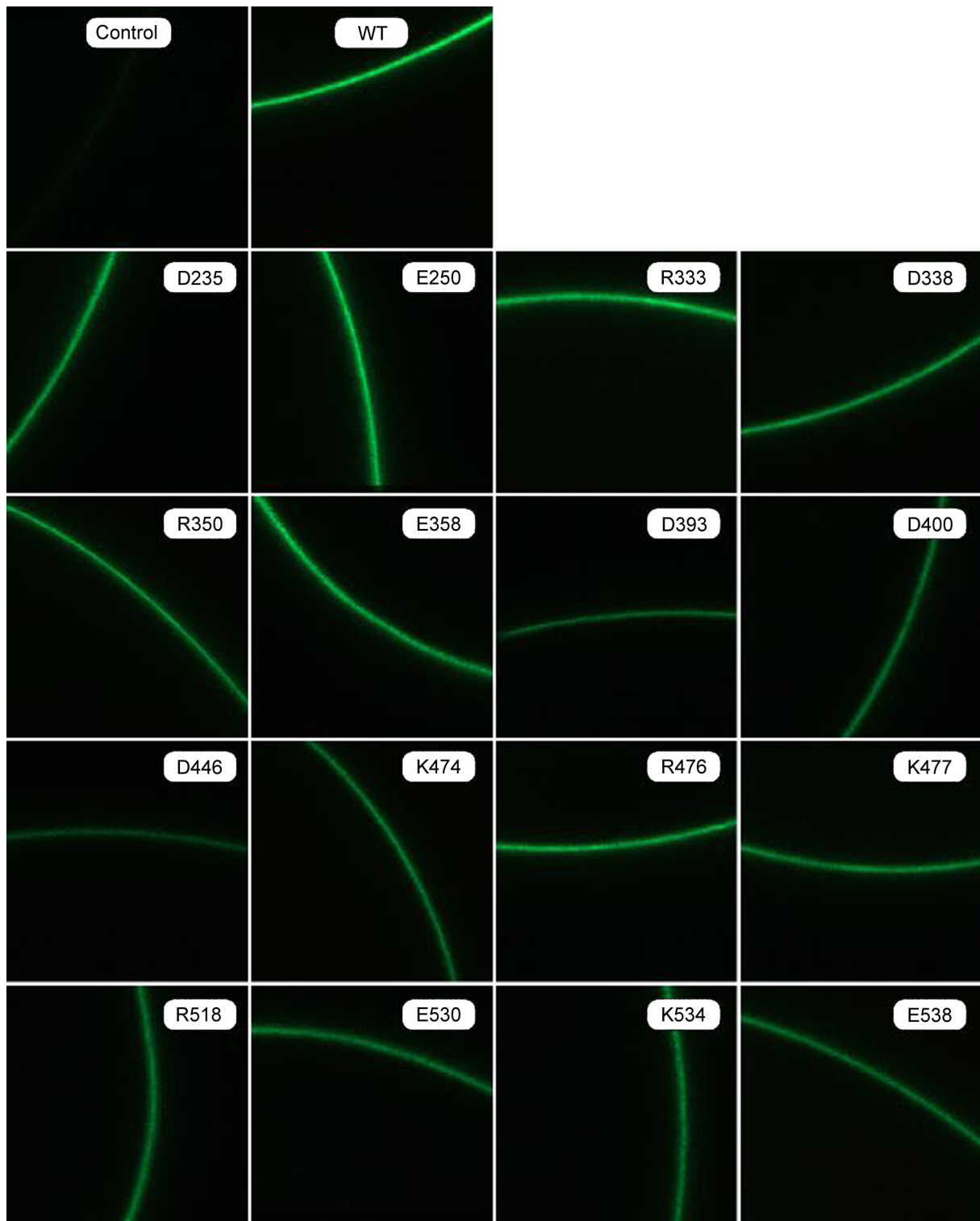


Fig. 8. Fluorescence micrographs of γ -ENaC-yellow fluorescent protein (YFP) hybrid protein expressed together with α - and β -ENaC subunits in the animal (dark) hemisphere surface of *Xenopus laevis* oocytes. The control oocytes were injected with only γ -ENaC-YFP and β -ENaC cRNAs. Other oocytes were injected either with WT or mutated α -ENaC cRNAs wherein the indicated α -ENaC residue was mutated to alanine. For other details, see METHODS.

Na⁺ self-inhibition effect provides an explanation for the discrepancy between cell surface expression and ENaC Na⁺ conductance activity. Three of the alanine mutants showed a major discrepancy between the cell surface density of ENaC and macroscopic conductance of ENaC. In other words, the

data for these mutants deviated from the linear regression line shown in Fig. 10. The combined results for the three parameters measured for these exceptional cases are shown in Fig. 11.

The most exceptional among these three mutants was the E250A mutation. The cell surface expression of this mutant

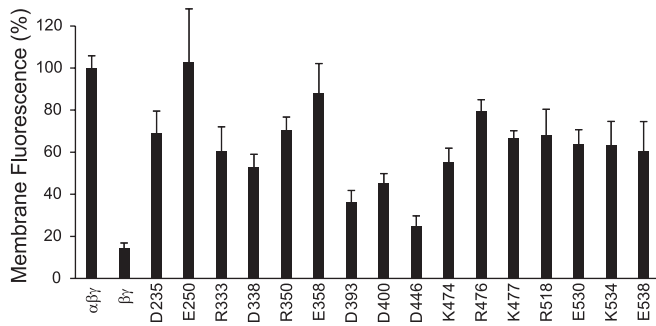


Fig. 9. Cell surface intensity of fluorescence of γ -ENaC-YFP hybrid protein expressed together with α - and β -ENaC subunits in *X. laevis* oocytes. The residue noted at the bottom of each bar was mutated to alanine. Each bar represents the mean \pm SE of at least 10 oocytes/residue. The fluorescence intensity was measured as noted in METHODS.

was similar to WT ENaC, but its Na^+ conductance was $<50\%$ of WT ENaC. The time constant for Na^+ self-inhibition for this mutant was $\sim 30\%$ of WT ENaC, and I_{ss}/I_{peak} was 40% of WT. These results together provide an explanation for the low activity of the mutant: a lower τ value means that the mutation enhances Na^+ self-inhibition; accordingly, a low I_{ss}/I_{peak} indicates a considerable decrease in P_o . Consequently, although the membrane density of the channel is as high as the WT ENaC, the channel does not work as efficiently as WT ENaC, resulting in lower Na^+ conductance. The R350A mutation showed a behavior similar to that of the E250A mutation.

The third case (D393A) showed a discrepancy that was the opposite of the two prior cases. The D393A mutant showed twofold higher Na^+ conductance than would be expected from its cell surface density (Fig. 11). However, the mutation greatly reduced Na^+ self-inhibition of ENaC (τ value ~ 2 -fold higher than WT, and $I_{ss}/I_{peak} \sim 140\%$ of WT). Thus, even though the membrane density of ENaC was low, the channels worked with greater efficiency and probably had a higher P_o (as a result of

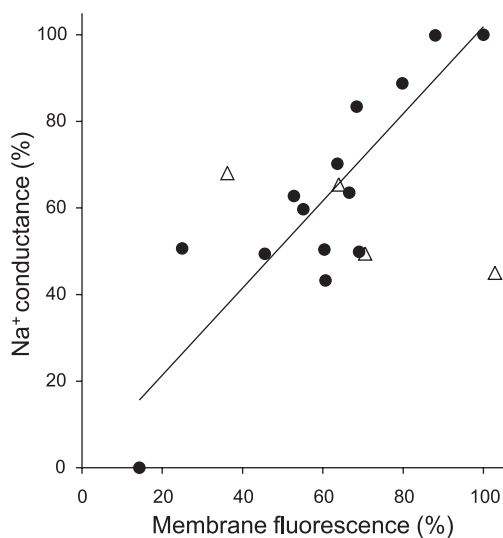


Fig. 10. Correlation of Na^+ conductance with oocyte cell surface fluorescence of ENaC. The points are taken from the results of the experiments shown in Figs. 2 and 9. Four residues (Glu250, Arg350, Asp393, and Glu530), mutations of which to alanine had the greatest effect on Na^+ self-inhibition, were excluded from the linear regression but are shown on the plot as open triangles. The Pearson correlation coefficient is $r = 0.87$ ($P < 0.0001$).

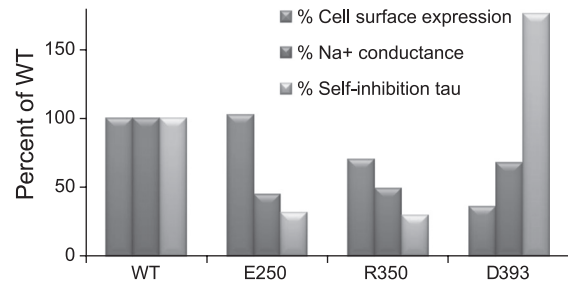


Fig. 11. Na^+ self-inhibition provides an explanation for the difference between cell surface expression and Na^+ conductance activity results for 3 mutants. The data for the 3 measured parameters were taken from the experiments shown in Figs. 2, 6, and 9.

lower Na^+ self-inhibition), enhancing the relative Na^+ conductance of ENaC.

In a similar vein, the E530A mutation greatly increased the τ value ($\sim 170\%$ of WT) and I_{ss}/I_{peak} ($\sim 130\%$ of WT). This increase was not associated with an apparent change in Na^+ conductance of ENaC, probably being counterbalanced by the 35% decrease in membrane expression level.

DISCUSSION

We undertook the present study to understand the roles of conserved charged residues in the ECD of ENaC, by mutating them to uncharged alanine and examining the activity of the mutated channels. A major initial concern in mutagenesis studies was that mutations may artificially disrupt normal folding of proteins, reflecting nonspecific effects beyond the location of the modified residue. To address this possibility, we selected residues exposed on the surface of ENaC based on the homologous ASIC1 crystal structure (Table 3). Thus their modification would be less likely to disrupt normal folding compared with residues located within the core of the protein. This assumption was supported by the finding that control mutations wherein the charge of the residue was maintained did not cause a significant change in ENaC activity (Fig. 3). Overall, our results revealed specific roles for selected residues consistent with their presumed structural locations.

Sodium conductance of the mutant forms of ENaC expressed in oocytes is commonly assayed using the two-electrode voltage-clamp method. The whole cell current measured by this method depends on both the number of the channels in the membrane and the P_o of each channel. To examine these two independent aspects, in addition to measuring ENaC activity, we also measured cell surface density of ENaC and Na^+ self-inhibition of ENaC. Our results revealed distinct correlations between the parameters assayed and elucidated the roles of specific charged residues in these processes.

Conserved charged residues on the surface of ECD take part in Na^+ self-inhibition of ENaC and/or trafficking to the membrane. Mutation of 12 of 16 conserved residues to alanine affected either Na^+ self-inhibition of ENaC and/or cell surface density of ENaC. Mutations of four residues (E250, R350, D393, and E530) most strongly affected Na^+ self-inhibition. Mutation of 12 of the 16 residues resulted in decreased cell surface expression of ENaC. Three residues mutated (D393, E530, and E538) appear to have dual roles, participating in both structures and interactions responsible for Na^+ self-inhibition as well as for trafficking to the cell surface. Among

the 16 mutations, only one (E250A) stands out as a mutation that did not affect cell surface expression but drastically enhanced Na^+ self-inhibition. Thus this residue appears to be involved solely in determining Na^+ self-inhibition, without playing a role in membrane trafficking. Overall, these results indicate that most of the charged residues are essential for trafficking of the subunits to the membrane or for their retention at the surface.

Effect of mutations on whole cell current could be accounted for by changes in membrane density of ENaC and Na^+ self-inhibition. For the specific mutants we studied, the decrease in ENaC activity could be accounted for by two determinants only: 1) effect of the mutation on cell surface density of ENaC, and 2) effect of the mutation on Na^+ self-inhibition. The effects of the mutations on ENaC activity could be categorized into three groups: 1) mutations that decreased ENaC activity mainly by decreasing membrane density of ENaC, 2) mutations that affected ENaC activity mainly by changing Na^+ self-inhibition of ENaC, and 3) mutations that affected both parameters to varying degrees. A strong correlation ($r = 0.87$) between membrane density and Na^+ conductance activity was observed for 12 mutants. Arbitrarily, we include these in the first group, although some of the mutations in this group had a small but significant effect on Na^+ self-inhibition as well. Only one residue (E250) is included in the second group. The comparative analysis presented in RESULTS and in Fig. 11 shows that the major effect of the E250A mutation on the activity of ENaC was via enhancement of Na^+ self-inhibition. For one mutation (D393A), we observed major contributions of both determinants. D393A mutation decreased Na^+ self-inhibition (increased τ), compensating for reduced membrane density.

In a study examining the role of cysteines in the ECD of mouse α -ENaC, some double mutants were observed to decrease Na^+ self-inhibition (34). These mutants were suggested to constitute a distinct group of “gain-of-function” mutations that enhance ENaC activity, different from the Liddle syndrome causing mutations in the PY motif that are involved in the ubiquitin-dependent degradation of ENaC (30). Since this study did not examine the effect of the mutations on ENaC cell surface density, we do not know whether these mutations would indeed increase ENaC activity. In our study, we identified two mutations that decrease Na^+ self-inhibition (D393A and E530A). However, our results show that mutations that affect Na^+ self-inhibition may also affect cell surface density. The final effect on ENaC activity would be determined by both of these parameters, as illustrated in Fig. 11. Thus our findings emphasize that reduction of Na^+ self-inhibition of ENaC may not necessarily be associated with enhanced ENaC activity.

The finding that single-residue mutations affect Na^+ self-inhibition raises the possibility that some cases of PHA and Liddle syndrome may be due to such mutations. However, none of the mutations generated in this study have been reported as a SNP or as a mutation responsible for PHA.

Location of mutated residues on the ENaC surface. To estimate the location of the mutated residues on the ENaC surface, we mapped the positions of the homologous residues on the structure of ASIC1 (16). Figure 12 shows the surface positions of four residues homologous to α -ENaC R350, D393, D400, and D446 (K247, D290, D297, and T337 in ASIC1).

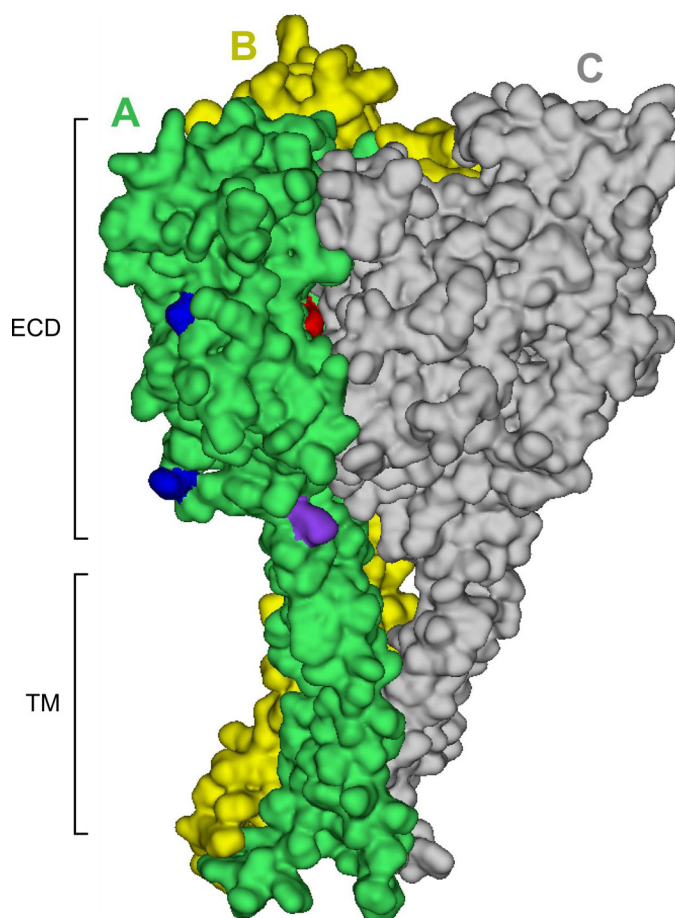


Fig. 12. Surface of homologous acid-sensing ion channel 1 (ASIC1) homotrimeric structure with selected residue surfaces marked in color. The letter marking indicates the color of each chain (A, B, and C). Only 4 residue surfaces have been color-marked on *chain A*. The homolog of α -ENaC R350 (K247, red) is visible through a pore on the ASIC1 surface between *chains A* and *C*. The homolog of α -ENaC D393 (D290, purple) is located close to *chain C*. The homologs of α -ENaC D400 and D446 (D297 and T337, blue) appear exposed on the surface. ECD, extracellular domain.

Alanine mutagenesis of these four residues showed the highest effect on surface expression and/or self-inhibition of ENaC (Figs. 6 and 9). One residue (E250) that also had a strong effect on self-inhibition of ENaC could not be mapped as it has no homolog in ASIC1. The homolog of α -ENaC R350 (K247, red in Fig. 12) is located just at the interface between *chains A* and *C* of ASIC1. Modification of R350 to alanine showed the greatest effect on Na^+ self inhibition (Fig. 6). Although this residue is located deeply between the two chains, it is visible through a pore on the ASIC1 surface in the orientation shown in Fig. 12. Incidentally, this residue is conserved in all three subunits of ENaC as well as chicken ASIC1 (Table 3).

The homolog of α -ENaC D393 (D290, purple in Fig. 12) is located at a site close to *chain C* on ASIC1. Its mutation to alanine resulted in strong effects on both cell surface expression and Na^+ self-inhibition. It should be noted that the N terminal of α -ENaC is cut by proteases, probably providing greater mobility to this segment. Thus this charged residue may play a critical role in ion permeation after cleavage of the subunit.

Finally, the homologs of α -ENaC D400 and D446 (D297 and T337, blue in Fig. 12) appear completely exposed on the

protein surface far removed from the other two chains (Fig. 12). The mutations of these two residues showed the strongest effect on cell surface expression but had no effect on self-inhibition. The lack of an effect on self-inhibition is explainable by the fact that these two do not appear on the path of ion permeation. Since self-inhibition reflects P_o , this result also indicates that once in the membrane, the modified channel functions normally, i.e., excluding the possibility of a misfolding in the protein. Mutation of these two aspartates should not affect subunit-subunit interactions as they do not appear in the interface between two chains. Thus the remaining alternative is that the mutations of these residues may have affected surface expression by interrupting interactions with other molecules during transport to membrane.

One interesting residue that is not visible in Fig. 12, as it is hidden between *chains A* and *C*, is the homolog of E538 (Q421 in ASIC1). In ASIC1 structure, this Gln421 appears to be involved in intersubunit interactions with Asp79 of *chain C* (16). Mutation of E538 affected both cell surface delivery and self-inhibition (Figs. 6 and 9). Thus this result indicates that both cell surface delivery and self-inhibition are strongly dependent on subunit-subunit interactions.

Mechanisms of effects of mutations on ENaC cell surface density. In epithelial cells, ENaC subunits are synthesized in the endoplasmic reticulum and transported specifically to the apical membrane facing the lumen. The route of transport of the subunits apparently proceeds via the Golgi complex and the trans-Golgi network. The proteins are then probably packaged in vesicular endosomes that are directed to the apical membrane (5, 36). Studies on a variety of apical proteins have revealed several alternative routes of vesicular trafficking (41). In some cell types, ENaC appear to be transported in membrane lipid raft domains (5).

The oocyte system used here is a heterologous expression system for human proteins encoded by our cDNA constructs. The possibility that the behavior of the proteins in human cells may be different cannot be ruled out. However, the fact that in oocytes all the subunits reach the membrane and together form a functional ENaC indicates that most aspects of the intracellular trafficking machinery are conserved in vertebrate cell types. In oocytes, as in epithelial cells, cell surface expression of ENaC is dependent on the expression of all three subunits (Figs. 8 and 9). Thus apparently all three ENaC subunits need to be "packaged together" for transport to the membrane. Thus it is possible that mutations that affect ENaC subunit-subunit interactions may weaken the interaction between subunits and reduce the efficacy of packaging of ENaC for surface delivery. This possibility can be examined in the future by generating complementary charged residue mutations on other ENaC subunits and switching positions of charged residues to reconstruct salt bridges.

Although the course of events that transports ENaC subunits to the apical membrane is not well understood, there is evidence that ENaC subunits bind and interact with proteins involved in directional trafficking to the membrane (15). These proteins include SNARE type proteins such as syntaxin (3), Rab GTPases (29), and G proteins (17). The list of proteins involved is probably longer than we currently recognize (41).

Salt bridges based on charged residues have been noted as the major participants in specific protein-protein interactions (23). Thus mutation of charged residues to Ala might have

possibly interrupted interactions with other proteins involved in sorting, packaging, or transporting ENaC subunits, leading to a significant reduction in the number of ENaC channels assembled in the membrane.

Cell surface expression of ENaC is regulated by diverse signaling molecules and proteins such as protein kinases (36). It is also possible that mutation of charged residues may affect the interaction of ENaC with such regulatory molecules that influence surface density of ENaC.

In conclusion, examination of the roles of charged residues on the surface of α -ENaC revealed that most of these affect the surface expression levels, probably by taking part in protein-protein interactions during the transport process. Our results also further support previous studies that Na^+ -dependent self-inhibition is a very significant determinant of ENaC activity.

ACKNOWLEDGMENTS

This work was carried out by O. Edelheit in partial fulfillment of the requirements for a PhD at the Sackler Faculty of Medicine, Tel Aviv University.

GRANTS

This research was funded in part by a grant from the Chief Scientist of the Israel Ministry of Health (to I. Hanukoglu and A. Hanukoglu) and by the generous contribution of the Peter Simpson Family Fund.

DISCLOSURES

No conflicts of interest, financial or otherwise, are declared by the authors.

REFERENCES

1. Antalis TM, Buzza MS, Hodge KM, Hooper JD, Netzel-Arnett S. The cutting edge: membrane-anchored serine protease activities in the pericellular microenvironment. *Biochem J* 428: 325–346, 2010.
2. Arnold K, Bordoli L, Kopp J, Schwede T. The SWISS-MODEL workspace: a web-based environment for protein structure homology modelling. *Bioinformatics* 22: 195–201, 2006.
3. Berdiev BK, Jovov B, Tucker WC, Naren AP, Fuller CM, Chapman ER, Benos DJ. ENaC subunit-subunit interactions and inhibition by syntaxin 1A. *Am J Physiol Renal Physiol* 286: F1100–F1106, 2004.
4. Berggren K, Wolf A, Asenjo JA, Andrews BA, Tjerneld F. The surface exposed amino acid residues of monomeric proteins determine the partitioning in aqueous two-phase systems. *Biochim Biophys Acta* 1596: 253–268, 2002.
5. Butterworth MB, Edinger RS, Frizzell RA, Johnson JP. Regulation of the epithelial sodium channel by membrane trafficking. *Am J Physiol Renal Physiol* 296: F10–F24, 2009.
6. Canessa CM, Schild L, Buell G, Thoresen B, Gautschi I, Horisberger JD, Rossier BC. Amiloride-sensitive epithelial Na^+ channel is made of three homologous subunits. *Nature* 367: 463–467, 1994.
7. Chang SS, Grunder S, Hanukoglu A, Rosler A, Mathew PM, Hanukoglu I, Schild L, Lu Y, Shinkets RA, Nelson-Williams C, Rossier BC, Lifton RP. Mutations in subunits of the epithelial sodium channel cause salt wasting with hyperkalaemic acidosis, pseudohypoaldosteronism type 1. *Nat Genet* 12: 248–253, 1996.
8. Chenna R, Sugawara H, Koike T, Lopez R, Gibson TJ, Higgins DG, Thompson JD. Multiple sequence alignment with the Clustal series of programs. *Nucleic Acids Res* 31: 3497–3500, 2003.
9. Chraïbi A, Horisberger JD. Na self inhibition of human epithelial Na channel: temperature dependence and effect of extracellular proteases. *J Gen Physiol* 120: 133–145, 2002.
10. Edelheit O, Hanukoglu A, Hanukoglu I. Simple and efficient site-directed mutagenesis using two single-primer reactions in parallel to generate mutants for protein structure-function studies. *BMC Biotechnol* 9: 61, 2009.
11. Edelheit O, Hanukoglu I, Gizewska M, Kandemir N, Tenenbaum-Rakover Y, Yurdakok M, Zajacsek S, Hanukoglu A. Novel mutations in epithelial sodium channel (ENaC) subunit genes and phenotypic ex-

- pression of multisystem pseudohypoaldosteronism. *Clin Endocrinol (Oxf)* 62: 547–553, 2005.
12. **Edelheit O, Hanukoglu I, Shriki Y, Tfilin M, Dascal N, Gillis D, Hanukoglu A.** Truncated beta epithelial sodium channel (ENaC) subunits responsible for multi-system pseudohypoaldosteronism support partial activity of ENaC. *J Steroid Biochem Mol Biol* 119: 84–88, 2010.
 13. **Hanukoglu A, Edelheit O, Shriki Y, Gizewska M, Dascal N, Hanukoglu I.** Renin-aldosterone response, urinary Na/K ratio and growth in pseudohypoaldosteronism patients with mutations in epithelial sodium channel (ENaC) subunit genes. *J Steroid Biochem Mol Biol* 111: 268–274, 2008.
 14. **Hanukoglu A.** Type I pseudohypoaldosteronism includes two clinically and genetically distinct entities with either renal or multiple target organ defects. *J Clin Endocrinol Metab* 73: 936–944, 1991.
 15. **Hille B.** *Ion Channels of Excitable Membranes*. Sunderland, MA: Sinauer, 2001.
 16. **Jasti J, Furukawa H, Gonzales EB, Gouaux E.** Structure of acid-sensing ion channel 1 at 19 Å resolution and low pH. *Nature* 449: 316–323, 2007.
 17. **Karpushev AV, Levchenko V, Pavlov TS, Lam VY, Vinnakota KC, Vandewalle A, Wakatsuki T, Staruschenko A.** Regulation of ENaC expression at the cell surface by Rab11. *Biochem Biophys Res Commun* 377: 521–525, 2008.
 18. **Kleyman TR, Carattino MD, Hughey RP.** ENaC at the cutting edge: regulation of epithelial sodium channels by proteases. *J Biol Chem* 284: 20447–20451, 2009.
 19. **Kumar S, Nussinov R.** Close-range electrostatic interactions in proteins. *Chembiochem* 3: 604–617, 2002.
 20. **Langloh AL, Berdiev B, Ji HL, Keyser K, Stanton BA, Benos DJ.** Charged residues in the M2 region of α -hENaC play a role in channel conductance. *Am J Physiol Cell Physiol* 278: C277–C291, 2000.
 21. **Liman ER, Tytgat J, Hess P.** Subunit stoichiometry of a mammalian K^+ channel determined by construction of multimeric cDNAs. *Neuron* 9: 861–871, 1992.
 22. **Maarouf AB, Sheng N, Chen J, Winarski KL, Okumura S, Carattino MD, Boyd CR, Kleyman TR, Sheng S.** Novel determinants of epithelial sodium channel gating within extracellular thumb domains. *J Biol Chem* 284: 7756–7765, 2009.
 23. **Musafia B, Buchner V, Arad D.** Complex salt bridges in proteins: statistical analysis of structure and function. *J Mol Biol* 254: 761–770, 1995.
 24. **Nicholas KB, Nicholas HB Jr., Deerfield DW II.** GeneDoc: analysis and visualization of genetic variation. *EMBnet.news* 4: 1–4, 1997.
 25. **Rossier BC, Pradervand S, Schild L, Hummler E.** Epithelial sodium channel and the control of sodium balance: interaction between genetic and environmental factors. *Annu Rev Physiol* 64: 877–897, 2002.
 26. **Rossier BC, Stutts MJ.** Activation of the epithelial sodium channel (ENaC) by serine proteases. *Annu Rev Physiol* 71: 361–379, 2009.
 27. **Sarakatsannis JN, Duan Y.** Statistical characterization of salt bridges in proteins. *Proteins* 60: 732–739, 2005.
 28. **Saxena A, Hanukoglu I, Strautnieks SS, Thompson RJ, Gardiner RM, Hanukoglu A.** Gene structure of the human amiloride-sensitive epithelial sodium channel beta subunit. *Biochem Biophys Res Commun* 252: 208–213, 1998.
 29. **Saxena SK, Kaur S.** Regulation of epithelial ion channels by Rab GTPases. *Biochem Biophys Res Commun* 351: 582–587, 2006.
 30. **Schild L, Lu Y, Gautschi I, Schneeberger E, Lifton RP, Rossier BC.** Identification of a PY motif in the epithelial Na channel subunits as a target sequence for mutations causing channel activation found in Liddle syndrome. *EMBO J* 15: 2381–2387, 1996.
 31. **Schild L.** The epithelial sodium channel: from molecule to disease. *Rev Physiol Biochem Pharmacol* 151: 93–107, 2004.
 32. **Sheng S, Bruns JB, Kleyman TR.** Extracellular histidine residues crucial for Na^+ self-inhibition of epithelial Na^+ channels. *J Biol Chem* 279: 9743–9749, 2004.
 33. **Sheng S, Carattino MD, Bruns JB, Hughey RP, Kleyman TR.** Furin cleavage activates the epithelial Na^+ channel by relieving Na^+ self-inhibition. *Am J Physiol Renal Physiol* 290: F1488–F1496, 2006.
 34. **Sheng S, Maarouf AB, Bruns JB, Hughey RP, Kleyman TR.** Functional role of extracellular loop cysteine residues of the epithelial Na^+ channel in Na^+ self-inhibition. *J Biol Chem* 282: 20180–20190, 2007.
 35. **Sheng S, McNulty KA, Harvey JM, Kleyman TR.** Second transmembrane domains of ENaC subunits contribute to ion permeation and selectivity. *J Biol Chem* 276: 44091–44098, 2001.
 36. **Snyder PM.** Minireview: regulation of epithelial Na^+ channel trafficking. *Endocrinology* 146: 5079–5085, 2005.
 37. **Stockand JD, Staruschenko A, Pochynyuk O, Booth RE, Silverthorn DU.** Insight toward epithelial Na^+ channel mechanism revealed by the acid-sensing ion channel 1 structure. *IUBMB Life* 60: 620–628, 2008.
 38. **Strautnieks SS, Thompson RJ, Hanukoglu A, Dillon MJ, Hanukoglu I, Kuhnle U, Seckl J, Gardiner RM, Chung E.** Localisation of pseudohypoaldosteronism genes to chromosome 16p122–1311 and 12p131-pter by homozygosity mapping. *Hum Mol Genet* 5: 293–299, 1996.
 39. **Valentijn JA, Fyfe GK, Canessa CM.** Biosynthesis and processing of epithelial sodium channels in *Xenopus* oocytes. *J Biol Chem* 273: 30344–30351, 1998.
 40. **Wang D, Voth GA.** Proton transport pathway in the CIC Cl^-/H^+ antiporter. *Biophys J* 97: 121–131, 2009.
 41. **Weisz OA, Rodriguez-Boulan E.** Apical trafficking in epithelial cells: signals, clusters and motors. *J Cell Sci* 122: 4253–4266, 2009.
 42. **Zhu ZY, Karlin S.** Clusters of charged residues in protein three-dimensional structures. *Proc Natl Acad Sci USA* 93: 8350–8355, 1996.